Determination of the number and size of inhomogeneities in thin films by ion beam analysis

J. P. Stoquert
Laboratoire PHASE (UPR 292 du CNRS), 23 rue de Loess, BP 20 CR, 67037 Strasbourg Cedex 2, France

T. Szörényi
Research Group on Laser Physics, Hungarian Academy of Sciences, P. O. Box 406, H-6701 Szeged, Hungary
(Received 28 January 2002; revised manuscript received 20 May 2002; published 29 October 2002)

Ion beam analysis techniques are routinely used to determine elemental concentration profiles in thin layers of thicknesses between tens of nanometers and micrometers. The analysis of the energy spreading of the analyzing ion beam, as described in this paper, represents a different approach to the determination of the dimension and number density of nanometer-size inhomogeneities in the films and opens interesting possibilities in the noninvasive characterization of film microstructure by ion beam techniques. The sensitivity of the method depends on the energy resolution of the detecting system: in usual configurations the presence of inclusions of dimensions down to a few nanometers can be detected. Procedures for calculation of the size and number density of spherical inclusions are presented. The case of columnar inhomogeneities is also described in detail and a parameter characterizing the degree of organization of the spatial distribution of inclusions is introduced. Examples of application in Rutherford backscattering spectroscopy, elastic recoil detection analysis, and nuclear reaction analysis reveal that the method described allows fast and accurate measurement without destruction of the samples in all cases. Comparison of feature dimensions derived from the analysis of the energy spreading with results of direct measurements, wherever possible, demonstrates the strength of the method.

DOI: 10.1103/PhysRevB.66.144108 PACS number(s): 82.80.Yc, 34.50.Bw, 61.18.Bn, 68.55.−a

I. INTRODUCTION

Ion beam analysis techniques, IBA, are effectively used for quantitative determination of both the absolute concentration and depth distribution of the constituting elements of thin films.[1] The ion beam detects the number of atoms in a layer of unit area (at./cm^2). By measuring the thickness using any other technique, the average density of the film material can be calculated, which, in comparison with the bulk material values, gives qualitative (mean) information on the homogeneity and compactness of the layer. The energy loss of the ions contains depth information. Therefore the analysis of the shape of the energy spectrum of the emitted ions yields information on the concentration profiles (concentration vs depth), in ideal cases with monolayer resolution.

Even when analyzing uniform, homogeneous films of flat, parallel surfaces, the depth resolution is limited by (i) the energy straggling and multiple-scattering effects within the sample,[2] and (ii) the characteristics of the experimental setup: the energy and angular spread of the analyzing beam, the geometric spread due to the finite beam size and detector aperture, the energy resolution of the detection system, and the response function of the absorber foils used.[3–5] In the case of real samples the depth resolution is further reduced by the energy spread from rough surface(s)[6–9] and inhomogeneities in thickness and volume.[10]

Clearly, this so-called structure-induced energy spread[3–5] sets a problem when interpreting the measured spectra. The effect of surface roughness on Rutherford-backscattering spectroscopy (RBS) and elastic recoil analysis (ERDA) spectra of nitrogen implanted carbon samples has been investigated both experimentally and by computer simulations (Ref. 8 and references therein). Itoh and co-workers have successfully reconstructed the surface structure of an optical grating from measured RBS spectra.[11] The code SURF, developed for the simulation of surface effects in ERDA, has been tested on an etched Si grid of 0.38 μm depth, 0.35 μm width, and 1 μm period, i.e., on a well defined periodic structure, as well.[7]

Although it has been recognized that the structure-induced energy spread component of the energy spectra contains valuable information on the real structure of the sample, the possibility of extracting structure information from the analysis of the energy spread has not been exploited yet. Early attempts to check foil thickness uniformity[10] and to determine thickness fluctuations[12] have demonstrated the potential of IBA. This surface characterization approach has been surpassed by more direct and convenient techniques, like scanning tunneling microscopy or atomic force microscopy. In the special case of (columnar) porous silicon it has been demonstrated that IBA methods are sensitive to the porous structure of the samples,[13–16] but the question of how to derive information on the microstructure of the film material from the analysis of IBA results in general remained a challenge.

The measurement of the number and size of inhomogeneities of submicron dimension embedded in a solid matrix is an extremely difficult task. Scanning transmission electron microscopy (STEM), for example, although offering the most direct way to get detailed information on such nanometer scaled structures, suffers the disadvantages of requiring fastidious preparation techniques, long handling times, and the risk of modifying the properties of the sample to be analyzed during preparation. Optical absorption, fluorescence, and magnetic measurements yield indirect information, if any, and need individual calibration for each type of material. Therefore there is a great demand for techniques allow-

ing simple and fast characterization of inhomogeneities at the nanometer level.

In this paper we show that the detailed analysis of the energy spreading of a beam going through a thin film provides quantitative information on the number and dimensions of the islands or voids traversed. Thus from the measured spreading and thickness it is possible to determine both the size (symmetry and diameter) and number density of the islands or voids within the film matrix. When knowing these figures, other parameters like the internal surface or the degree of self-organization can also be deduced. The method presented is general in the sense that it can be applied to any kind of domains isolating different materials or the same material of different density (e.g., gas bubbles, voids) embedded in an otherwise homogeneous matrix, which we will hereinafter refer to as ''inclusions'' for brevity. Calculations for the cases of spherical and columnar structures are detailed in the appendices.

II. PRINCIPLE OF CALCULATION

Consider a thin layer of thickness e, the matrix, in which spheres of constant radius R and of different material are embedded (Fig. 1). Two materials are considered to be different if they do not have the same stopping power, i.e., if they have different elemental composition and/or density.

An ion beam of mean incident energy E_i and outgoing energy E_o passes the layer. The number of inclusions per unit volume is N (cm^{-3}) and the mean number N' of inclusions traversed by an incident ion is $N' = N \cdot \pi R^2 \cdot e/\cos\theta_i$. The mean path length inside a spherical inclusion is $\overline{l} = 4R/3$. With e_g being the projection of the total length traversed inside the inclusions to the normal of the surface F, the fraction of the total volume occupied by the inclusions, which is equal to the fraction of the path inside inclusions, is

$$F = \frac{e_g}{e} = N\frac{4}{3}\pi \cdot R^3. \tag{1}$$

The thickness $e = e_m + e_g$ (the indices m and g stand for matrix and inclusions, respectively) is related to the energy loss $\Delta E = E_i - E_o$ (Fig. 1) and

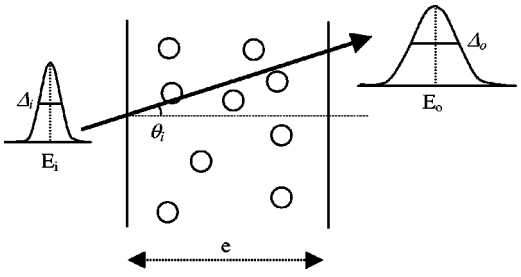

FIG. 1. The principle of a measurement in transmission geometry. Δ_i and Δ_o are the full width at half maximum (FWHM) of the energy distribution of the incoming and outgoing ion beams, respectively.

$$F = \frac{\dfrac{S_m}{\cos\theta_i} - \dfrac{\Delta E}{e}}{\dfrac{S_m - S_g}{\cos\theta_i}}, \tag{2}$$

When knowing the elemental composition of both the matrix and the inclusions [and thereby their stopping powers S (Ref. 17) and bulk atomic densities n], one can calculate the volume fraction F of the inclusions by measuring $\Delta E, \theta_i$ and the total thickness e. Equation (2) applies for any mixture of atoms or molecules of types m and g of mean densities $n_g e_g/e$ and $n_m e_m/e$ (cm^{-3}), independently of the size of the inclusions. This is the traditional way to use IBA. Furthermore, an independent thickness value e also allows us to check that the analyzed layer is actually a mixture (which may also be a matrix with inclusions below the limit of resolution) or a compound.

The dimensions of inclusions are deduced from the measurement of the energy spreading. To this end, we consider statistical fluctuation around the mean value e_g. For an incident monoenergetic beam of energy E_i, the outgoing particles are distributed around the mean energy E_o with a standard deviation Ω characterizing the energy spreading. For a perfectly parallel layer containing uniformly distributed atoms of only one type, i.e., without inclusions, the spreading Ω_n is the consequence of (i) the statistical fluctuations in the interactions responsible for the slowing down of the particles[2]—straggling and multiple scattering—and (ii) the experimental spreading,[3–9] as described in detail in Appendix A. When inclusions are embedded in the layer, another contribution to the spreading, Ω_g, must be taken into account,[13] that is due to the statistical fluctuation in the number of encounters with these inclusions. From the recorded spectrum the total spreading Ω ($\Omega^2 = \Omega_n^2 + \Omega_g^2$) can be determined, and Ω_g can be deduced after either estimating Ω_n from theoretical formulas[3] or measuring Ω_n on a layer without inclusions.

N' being the number of inclusions traversed by an ion and $\overline{l} = 4R/3$ the mean path in each inclusion, the mean path fluctuation in the inclusions is given by $\sigma(e_g) = \sqrt{N'}\frac{4}{3}R$. To calculate the corresponding variations in the energy losses in the thin layer, we have to take into account that an increase in path length in the inclusions implies a concomitant decrease in path length in the matrix, therefore $\sigma(\Delta E) = \Omega_g = |S_m - S_g|\sigma(e_g)$ or

$$\Omega_g^2 = \frac{1}{\cos\theta_i}(S_m - S_g)^2 \frac{4}{3} FRe. \tag{3}$$

By determining the fraction of the volume, F occupied by the inclusions [Eq. (2)] and the spreading Ω_g, the diameter R and the number N of the inclusions in the layer can be calculated by solving the system of Eqs. (1) and (3):

$$R = \frac{3}{4}\frac{\Omega_g^2 \cos\theta_i}{(S_m - S_g)^2 Fe},$$

$$N = \frac{3}{4}\frac{F}{\pi R^3}. \quad (4)$$

Equation (4) represents a first-order approximation in the case of a transmitted beam. Detailed calculations are given in Appendix A. Note that by this method it is possible to measure the number and size of inclusions below the instrumental limit of resolution. In nuclear measurements, we generally have to consider incoming and outgoing particles and the exact formulas for each technique (RBS, ERDA, or NRA) are given in Appendix A. Depending on the particular situation, IBA also provides a variety of possibilities to experimentally determine the mean concentrations and the F factors (peak area, peak height), which will not be detailed here. In the following, we will restrict ourselves to F calculations of the type given by Eq. (2).

III. EXPERIMENT

A. Experimental setup

For the determination of the number and dimension of the inclusions conventional IBA setups can be used without any modification or additional equipment. Clearly, special care has to be taken to the resolution of the detecting system in order to maximize the precision of structure induced spreading determination as discussed in Appendix A. For hydrogen measurements by ERDA a setup installed at the 4-MV Van de Graaff accelerator in Strasbourg was used. Here an incident ^{4}He ion beam of 2.9 MeV enters the target chamber containing a computer controlled manipulator with up to 35 samples. The angle of incidence with respect to the target normal is 80° and the detector, with a Mylar® film of 13 μm thickness in front of it, absorbing all scattered and recoiling atoms except hydrogen, is placed at 20° relative to the incident direction. The energy resolution of the silicon surface barrier detectors is 15 keV. The diameter of the incident beam is 1 mm, with an energy spread of 4 keV and angular spread of 0.05°. The detector to target distance is 100 mm and the diameter of the detector diaphragm is 3 mm.

The measurement data are represented in the classical way by plotting the number of ions recorded by the detecting system (detector + absorber) versus energy. The spreading Ω_g and the mean energy ΔE are extracted from these energy spectra.

B. Data analysis

For transmission geometry, as illustrated in Fig. 1, the energy distribution of the incoming (i) and outgoing (o) particles can be approximated by Gaussian functions with full width at half maximum (FWHM) Δ and standard deviations $\sigma(\Delta = 2.355\sigma)$. The spreading due to the inclusions is given by $\Omega_g = \sqrt{\sigma_o^2 - \sigma_i^2 - \Omega_n^2}$ where Ω_n—as defined previously—is the spreading for a perfect layer with all atoms uniformly distributed and with the same mean composition as the actual matrix containing the inclusions.

Figure 2 illustrates a typical spectrum recorded in reflection geometry. It is usual in IBA data analysis to adjust the two sides of the peak by error functions generated by convolution products of Gaussian functions with step functions. Δ_i and Δ_o are usually determined by taking the energy interval corresponding to 12–88% of the total height on each side of the plateau, though numerical simulations may yield more precise values. In a first approximation, Ω_n can be calculated by using Bohr's formula[2] for the straggling. More sophisticated calculations may result in more precise determination of the experimental[3–9] and theoretical[18–22] contributions to Ω_n, as detailed in Appendix A. In practice, σ_i is due to the spreading contributions from the beam, geometry, and stopper foil whereas σ_o, in addition, contains the depth dependent spreading caused by the straggling, multiple-scattering, path length difference and energy dependence of the stopping power. Both σ_i and σ_o are determined experimentally, and therefore only the depth dependent spreading has to be taken into account in Ω_n. For a sufficient precision of the final result Ω_n must not constitute the main contribution to the measured spreading. In the case of a spectrum exhibiting two peaks, corresponding to the matrix and to the inclusions, respectively, the volume fraction of the inclusions F and the spreading Ω_g can be measured simultaneously in different ways and redundant information is available in the experimental data.

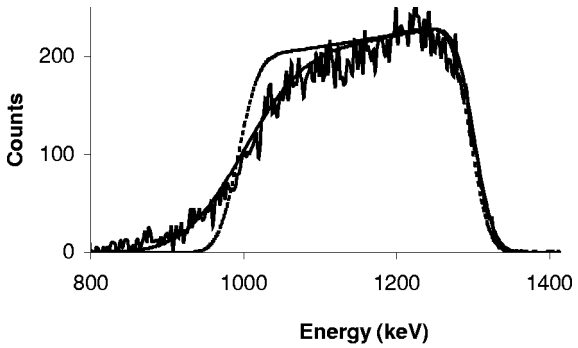

FIG. 2. Depth distribution of hydrogen within a carbon nitride film fabricated by ablation of a graphite target with ArF excimer laser pulses of 7.5 J cm^{-2} in an N_2 atmosphere of 50 Pa. Bold, continuous line: experimental ERDA spectrum; dotted line: simulation taking into account Bohr straggling; continuous line: simulation taking into account the structure-induced spreading due to spherical inclusions.

IV. EXAMPLES OF APPLICATION

A. Elastic recoil detection analysis

As reported earlier, ERDA revealed marked differences in both the total atomic concentration and the depth profile of hydrogen in carbon nitride films fabricated by ablating a graphite target in N_2 atmosphere of pressures between 10^{-2} and 100 Pa.[23] Relatively high hydrogen contents (12.8–16.45 at. %), uniformly distributed throughout the whole thickness, and low density values characterized the films deposited in the 50–100-Pa pressure domain (Fig. 2). In the case of these films surprisingly large values of the energy spreading parameter were necessary to fit the experimental

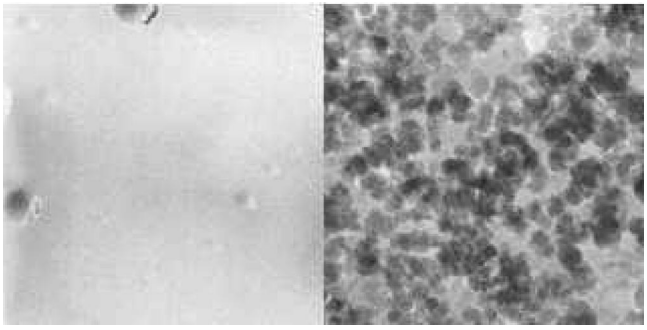

FIG. 3. TEM micrographs taken on carbon nitride films deposited with 10- $J\,cm^{-2}$ pulses in 5-Pa N_2 (left) and with 7.5-$J\,cm^{-2}$ pulses in 50-Pa N_2 (right). Each picture is 1×1 μm^2 in size.

data, indicating large fluctuations in the ion paths, i.e., large inhomogeneities in the analyzed layers.

Supposing that the layer of mean composition $CN_{0.32}H_{0.21}$ characterized by the spectrum shown in Fig. 2 is made of randomly distributed spherical clusters of constant radius R, Eq. (A2) given in Appendix A yields 82 nm for the mean diameter of the clusters, and a number density of 1.9×10^{15} voids/cm^3, corresponding to an internal surface of 39 m^2/cm^3. The smallest detectable diameter can be evaluated by assuming that the minimum detectable structure induced spreading is given by $\Omega_g=\Omega_{\min i}=\sqrt{\sigma_i^2+\Omega_n^2}$. Inserting this value in Eq. (A2), we obtain a minimum measurable diameter of 18 nm. The uncertainty of the measurement is evaluated to be 30%, as detailed in Appendix A, by taking an error of 10% on the total thickness e and of 10% on Ω_g^2 after determination of Ω_n with the code DEPTH.[3] Parallel TEM studies revealed that the above analysis of the ERDA spectra resulted in a both qualitatively and quantitatively correct description of the microstructure.[24] As exemplified in Fig. 3, at low pressures morphologically uniform, continuous films are grown and no inclusions were detectable in the ERDA spectra, while the film deposited at 50 Pa is composed of carbon nitride cluster agglomerates forming a porous structure. The dimension of both the cluster agglomerates and the voids between them ranges from several tens to more than 100 nm,[24] revealing that the mean diameter value 82 ± 25 nm, calculated from the ERDA spectrum, is a reliable average figure, indeed.

B. Nuclear resonant reaction

In a detailed study of porous silicon decorated with light elements (C,N,O,H) Amsel *et al.*[13] have shown that the morphology can be well characterized by recording rocking curves, and the anisotropy effects have been evidenced by comparison of spongelike (with spherical pores) and columnar films. From measured data of proton energy-loss fluctuations in ^{15}N decorated porous layers with the narrow resonance at 430 keV of the $^{15}N(p,\alpha\gamma)^{12}C$ reaction, as given in Ref. 13, we have calculated explicitly the diameter and density of the columns that characterize the nanometric structure, using a formalism developed for the columnar structure (cf. Appendix A.3.). The experimental data and the calculated values are compiled in Table I.

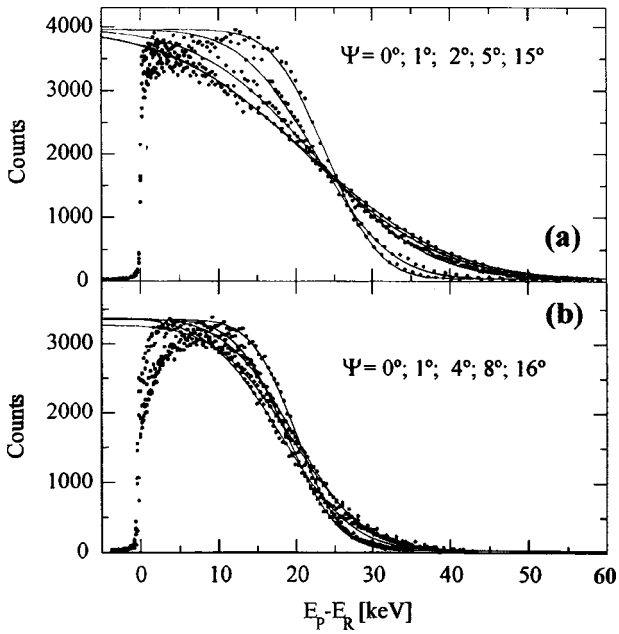

FIG. 4. $^{15}N(p,\alpha\gamma)^{12}C$ NRA excitation curves reprinted from Ref. 13, with permission from Elsevier Science, of a porous silicon columnar structure nitrided with ^{15}N: (a) at 1000 °C during 5 min., (b) at 1000 °C during 30 min., revealing transformation from a chaotic structure characterized by an order parameter $K=0.23$ to a highly organized structure with $K=K_c=0.08$.

Both the diameter and the area density of the pores calculated using the dense medium approach (Appendix B) with an order parameter $K=K_c=0.08$ characteristic of a high level of organization compare favorably to the estimations from the TEM image reported in Fig. 1 of Ref. 13. Table 2 in Ref. 13 compares spreading values in Bohr units for columnar and spongy films. The angular dependence is clearly seen

TABLE I. Structural features of a columnar porous silicon film of thickness 0.8 μm and mean composition $SiN_{0.6}O_{0.5}C_{0.32}H_{0.53}$, as calculated from experimental data given in Ref. 13. θ_i: angle of incidence; ΔE: mean energy loss; Ω: total straggling; Ω_c: structure induced straggling; R: column radius; N: surface density of colums; s_i: internal surface.

θ_i(°)	ΔE(keV) (Ref. 13)	Ω(keV) (Ref. 13)	Ω_c(keV) (Ref. 13)	$2R$(nm)	N(cm^2)	s_i(m^2/cm^3)
2	25,4	9,2	8,9	10,5	7.4×10^{11}	24,5
4	25,9	7,1	6,7	12,0	5.6×10^{11}	21,2
8	26,2	5,7	5,1	14,1	4.1×10^{11}	18
16	26,6	4,8	4,0	16,5	3.0×10^{11}	15,5
30	29,8	4,1	3,1	16,1	3.1×10^{11}	15,8

in the first case and does not appear in the second one, allowing for characterization of the anisotropy. Our calculations for spherical and cylindrical pores [Eqs. (A2) and (A3)] confirm these variations. Moreover, by analyzing the data given in Figs. 4(a) and (b) (reproduced from Ref. 13), the evolution of the order in the columnar system investigated can be followed. Figure 4(b) corresponds to a film nitrided at 1000 °C during 30 min. When calculating mean values for a dense columnar system with $K=K_c=0.08$ (maximum organization as shown in Appendix B) we obtained 11 nm for the diameter and $7.8\times10^{11}\mathrm{cm}^{-2}$ for the areal density, in agreement with previous results. Using these values for comparison with Fig. 4(a), $K=0.23$ is obtained for the film nitrided at 1000 °C during 5 min. This figure is between 1 and K_c, indicating a higher randomness in this case, demonstrating that the heat treatment increases the order in the columnar structure.

C. Rutherford backscattering spectroscopy

Experimental RBS spectra recorded on porous silicon samples can also be analyzed by our technique. IBA techniques have usually been used to determine elemental composition.[25] In Fig. 5 simulated RBS spectra of a perfect layer without inclusions and a porous one, with spherical pores of radius $4.5(\pm2)$ nm, an internal surface of 200 $\mathrm{m}^2/\mathrm{cm}^3$, and a randomness parameter $K=1$ are compared. The (unoptimized) measurement conditions correspond to those referring to Fig. 2 in Ref. 26. In this figure the effect of structure-induced spreading is clearly visible. We have also analyzed the RBS data given in Ref. 13 for a columnar porous silicon film of thickness 0.8 μm and mean composition $SiN_{0.6}O_{0.5}C_{0.32}H_{0.53}$. A diameter of 11 nm and an areal density of $6.7\times10^{11}\mathrm{cm}^{-2}$ have been found in this case (with $K=K_c=0.08$), in good agreement with the other measurements, showing the consistency of the results obtained by analyzing experimental data originating from different IBA techniques and TEM images.

V. CONCLUSION

The analysis of the energy spreading of the ion beam represents a different approach to the determination of the dimension and number density of nano-size inhomogeneities in thin films. The method described opens up interesting possibilities in the noninvasive characterization of film microstructure by IBA techniques. The sensitivity of the method depends on the energy resolution of the detecting system. In usual IBA configurations the presence of inclusions of sizes down to a few nanometers can be detected.

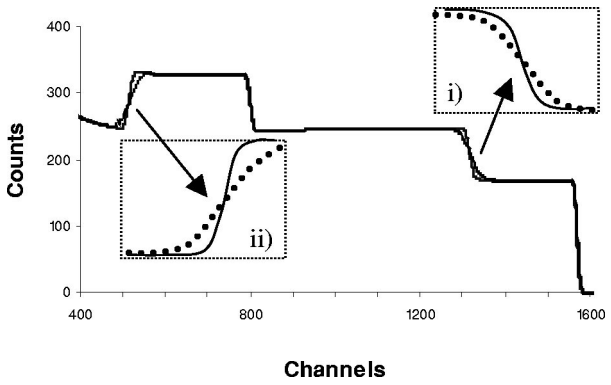

FIG. 5. Comparison of simulated RBS spectra of a dense (continuous line) and a porous layer (dotted line) of $SiC_{0.65}H_{0.66}$. Insets show the spreading due to porosity on (i) the silicon peak originating from the substrate and (ii) the carbon peak from the layer.

Algorithms for the calculation of the size and number density of spherical inclusions of constant radius R are given in detail (Appendix A). It is also shown that the calculations can be extended to the case of films containing inclusions with known distributions of radii R or, at least, errors can be estimated if these distributions are not known exactly. The case of columnar inhomogeneities is also described in detail, and a parameter between 0 and 1 characterizing the spatial order is introduced (Appendix B).

Examples of application demonstrate the strength of the method. The good agreement between the calculated figures and the parameters derived from (mostly TEM) measurements reveals that the method described is particularly promising, because it allows fast measurement without destruction of the samples and the procedure applies equally well to RBS, ERDA, and NRA. Forthcoming systematic studies to determine the optimal experimental conditions could help to promote it as a powerful tool of mesoscopic physics. Successful applications might excite renewed interest for theoretical and experimental work on energy spreading in relation with self-organization, as well.

ACKNOWLEDGMENTS

This research was partially supported by NATO's Scientific Affairs Division in the framework of the Science for Peace Program (SfP–971934), and by the Hungarian Ministry of Education & Le Ministere des Affaires Etrangeres within the framework of the bilateral intergovernmental S&T agreement between Hungary and France (TéT F-26/00).

APPENDIX A: GENERAL FORMULAS AND CORRECTIONS

1. General formulation for spherical inhomogeneities

Actual measurements are generally not performed in transmission geometry, to which the calculations presented refer, but in reflection geometry (Fig. 6). For that configuration, with E_i and E_o being the energies of incoming and outgoing particles, we define for all IBA techniques (Fig. 6) the following general notations:

$$\Delta E = kE_i - E_o = \{S\}_m e_m + \{S\}_g e_g ,$$

$$\{S\} = \frac{k}{\cos\theta_i} S_{in} + \frac{1}{\cos\theta_o} S_{out} ,$$

$$\Delta S = S_m - S_g ,$$

$$\{\Delta S\} = \{S\}_m - \{S\}_g ,$$

$$[\Delta S]^2 = \left[\frac{k^2}{\cos\theta_i} (\Delta S)^2_{in} + \frac{1}{\cos\theta_o} (\Delta S)^2_{out} \right],$$

where k is the kinematic factor ($k=\partial E_o/\partial E_i$ for an infinitely thin layer), and where indices m and g are introduced for the matrix and inclusions, respectively, in $k,\Delta E$, $\{S\}$, and $[\Delta S]$ where appropriate. Note please that care has to be taken: here S and $\{S\}$, as well as $\Delta S=(\Delta S)$, $\{\Delta S\}$ and $[\Delta S]$ have not the same meaning. Rewriting Eqs. (2) and (3) we obtain

$$F=\frac{\{S\}-\dfrac{\Delta E}{e}}{\{\Delta S\}}=N\frac{4}{3}\pi R^3,$$

$$\Omega_g^2=[\Delta S]^2F\frac{4}{3}Re. \tag{A1}$$

From Eq. (A1) R and N are easily deduced, knowing all other quantities. In practice, the determination of R and N necessitates the measurement of the mean energy loss ΔE and the energy spreading Ω by IBA techniques, and an independent determination of the total thickness e. Many situations can be analyzed: inclusions or voids in a matrix, cavities containing a gas, decorated voids, powder containing or decorated with different elements. Any nuclear technique can be used, resonant nuclear reactions being particularly attractive, because for sufficiently sharp resonances, the energy resolution of the detecting system can be ignored and the sensitivity to smaller radii is mostly limited by the intrinsic straggling estimated with Bohr's formula. Therefore it is advisable to use heavy ions and grazing angle geometries to optimize the experimental conditions. For example, an estimation made for the $^1\mathrm{H}(^{15}\mathrm{N},\alpha)^{12}\mathrm{C}^*\rightarrow{}^{12}\mathrm{C}+\gamma$ reaction at an angle of incidence of 80° shows that the method is potentially applicable for R values in the nanometer range.

The internal surface per unit volume (cm^{-1}) $s_i=3(F/R)$ can also be deduced from the experimental data. For nanometric inclusions, classical IBA gives only access to the (apparent) mean concentration of element g in the matrix m by analyzing the height of the peaks. The comparison of this value with that deduced using the method described here can give additional information on the internal structure of the layer.

2. Corrections and errors for spherical inhomogeneities

Throughout the above discussion we supposed that the contribution from the inclusions to the spreading is due to the fluctuation in the number of encountered inclusions, and that the path inside each inclusion is constant and equal to the mean path $\overline{l}=4R/3$. In the inclusions, however, there is also a fluctuation in the path l relatively to the mean path $\overline{l}$: $\sigma^2(l)=\overline{(l-\overline{l})^2}=\frac{2}{9}R^2$, and $\sigma^2(e_g)=N'[\overline{l^2}+\sigma^2(l)]=2N'R^2$, which adds a correction of 6% to the result of the previous calculations. Therefore Eq. (A1) rewrites:

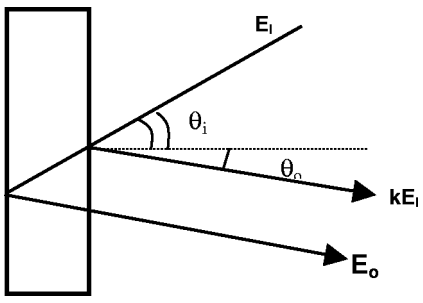

FIG. 6. Reflection geometry.

$$F=\frac{\{S\}-\dfrac{\Delta E}{e}}{\{\Delta S\}}=N\frac{4}{3}\pi R^3,$$

$$\Omega_g^2=[\Delta S]^2F2Re. \tag{A2}$$

The value of F is not affected by this correction, but the radius diminishes by 11% and the number of voids increases by 42%. In practice, if we consider spherical inclusions, formula (A2) has to be used.

These calculations are made on the presumption that all voids have the same radius R. A distribution in R will contribute to the spreading in a way which is similar to the one obtained in the previous case (distribution around $\overline{l}$). If we consider for example that the radii of the inclusions are uniformly distributed between $R/2$ and $3R/2$, the calculations according to Eq. (A2) overestimate R by 8% and underestimate the number of inclusions yielding an estimation of the reliability of the results. Even in very unfavorable cases the dimensions are correctly approximated by our method, and the initial hypothesis of spherical inclusions with constant radius R does not constitute a strong limitation of the method. Moreover, similar calculations can be applied for the characterization of any kind of domains defined by their first and second moments.

Besides the contributions from the inclusions discussed above, there are a number of other contributions to the energy spreading which are described in detail in Ref. 3. The code DEPTH (Ref. 3) allows for precise determination of these contributions for specific experimental conditions, together with the straggling of the ions calculated following Bohr[2] or Chu.[21] We recommend to use this code for the determination of Ω_n.

Surface and interface roughness give also rise to an additional energy spreading, which can be estimated by Monte Carlo simulations[7–9] or by means of analytical expressions.[10–12] Taking σ_r as the mean standard deviation characterizing the roughness, the corresponding energy spreading Ω_r behaves as $S\sigma_r$ and can be included in Ω_n by quadratic summation. In the cases described in the text, we obtain $\Omega_r^2=\{(1-F)^2[\Delta S]^2/\cos\theta\}\sigma_r^2$, with $\theta=\theta_i$ for ERDA and NRA and $\theta\approx\theta_i\approx\theta_o\approx 0$ for RBS. In particular, this contribution can be ignored if $\sigma_r^2\ll[2FRe/(1-F)^2]\cos\theta$, which shows also that in most practical cases, the roughness does not contribute to the energy spreading if the surface/interface irregularities are not significantly greater than the radius of the inhomogeneities.

Finally, using Eq. (A1) and neglecting the uncertainties on stopping powers, the total error on R can be calculated from the uncertainty of the energy spreading, taking into account the previous corrections, and from the uncertainty of the total thickness e, determined by the actual (non-nuclear) measure-

ment. As N depends mainly on $1/R^3$, the precision is poorer on the number than on the size of the inclusions, and these errors partially compensate each other in the determination of the internal surface.

3. General formulas for columnar inhomogeneities

The previous calculations apply to inhomogeneities of spherical shape. Another case of practical interest is the columnar structure, which can also be characterized by our method. Consider a structure with identical columns of diameter R inclined by an angle α with respect to the normal to the surface, to be measured using transmission geometry (Fig. 7). N represents now the surface density of the columns (cm^{-2}), the other notations being unchanged. The mean path in a column is

$$\overline{l}=\frac{\frac{\pi\cdot R^2 e}{\cos\alpha}}{\pi\cdot R^2\frac{\cos\theta_i}{\cos\alpha}+2Re\,\sin(\theta_i-\alpha)},$$

the mean number of crossed columns

$$N'=N\frac{\pi\cdot R^2\frac{\cos\theta_i}{\cos\alpha}+2Re\,\sin(\theta_i-\alpha)}{\cos\theta_i},$$

and the total mean path in the columns

$$N\frac{\pi\cdot R^2}{\cos\alpha}\frac{e}{\cos\theta_i}.$$

Equation (A1) rewrites (for $\theta_i\neq\alpha$):

$$F=N\frac{\pi\cdot R^2}{\cos\alpha},$$

$$\Omega_c^2=(\Delta S)^2\frac{N}{\cos\theta_i}\frac{\left(\frac{\pi\cdot R^2 e}{\cos\alpha}\right)^2}{\left[\pi\cdot R^2\frac{\cos\theta_i}{\cos\alpha}+2Re\,\sin(\theta_i-\alpha)\right]}. \tag{A3}$$

where $\Delta S=S_m-S_c$. The fraction of path in the columns is equal to the volume fraction occupied by the columns,

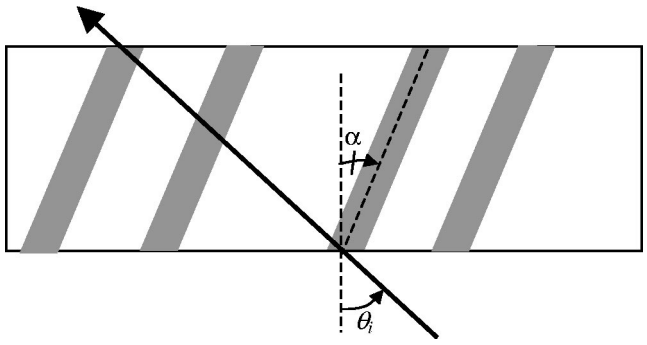

FIG. 7. Geometry in the case of a transmitted beam and columnar inhomogeneities.

and—as in the case of spherical inclusions—Eq. (2) can be used to determine F, and Eq. (A3) to calculate R and N.

These equations with $\alpha=0$ and $S_c=0$ have been used in Sec. IV B for the calculation of the diameter and density of columns perpendicular to the surface in porous silicon analyzed by a nuclear resonant reaction. For small angles of incidence with respect to columns orientation $[\theta_i-\alpha<(\pi/2)(R/e)]$ this statistical treatment cannot be adapted and the calculations do not apply.

4. Corrections and errors for columnar inhomogeneities

Equation (A3) can be generalized to include the case of reflection geometry

$$F=\frac{\{S\}-\frac{\Delta E}{e}}{\{\Delta S\}}=N\pi\cdot R^2,$$

$$\Omega_c^2=k^2\frac{A_i}{B_i+\frac{C_i}{R}}+\frac{A_o}{B_o+\frac{C_o}{R}} \tag{A4}$$

with $A=(\Delta S)^2 Fe/\cos\theta$, $B=\cos\theta/(e\cos\alpha)$, $C=(2/\pi)\sin(\theta-\alpha)$ (where ΔS_{Ei}, θ_i and ΔS_{Eo}, θ_o characterize the incoming and outgoing beams, respectively, as defined Fig. 6).

If $(\pi/2)(R/e)\ll\sin(\theta_i-\alpha)(\cos\alpha/\cos\theta_i)$ (which is generally the case if the direction of the incident beam is not parallel to the column orientation) these equations simplify and the corrections can be estimated similarly to the case of spherical inclusions. They are 4% for R if we replace $\overline{l^2}$ by $\overline{l}^2$, the other corrections[3] being the same for all types of inclusions.

Comparing the equations related to the spherical and columnar cases a difference in the angular dependence is apparent, which allows for experimental distinction between the two forms of the inhomogeneities by varying the angle of incidence.

APPENDIX B: ENERGY SPREADING AND SELF-ORGANIZATION

In all calculations we have supposed that the columns (or inclusions) are randomly distributed, i.e., their concentration is low enough to insure statistical independence. For high densities of inhomogeneities this assumption does not remain valid anymore, and the problem has to be reconsidered. In $\sigma^2(e_c)=N'[\overline{l^2}+\sigma^2(l)]=N'\overline{l^2}$ the two terms have different statistical meanings. The first one, which is a Bohr-type spreading, is due to the statistical fluctuations of the number of encounters with inclusions: $\sigma^2_{N'}(e_c)=N'\overline{l^2}$, the mean path remaining constant and equal to $\overline{l}$ in each collision. The second term, $\sigma_l^2(e_c)=N'\sigma^2(l)$ corresponds to a constant number of collisions, while the path in each inclusion is fluctuating.

In the case of statistical independence (Appendix A), we have shown that the second term represents a correction which has been calculated and taken into account. In the case of high densities of inclusions or columns, the limited avail-

able space induces some kind of ordering in the relative positions of the inclusions or columns, the spreading being the experimental manifestation of this chaotic, but not random-type organization. To approximate this particular situation, we consider only the second contribution to the spreading, related to the mean path fluctuation, the number of encountered entities being constrained to be constant. Calculations made in this approximation lead to the following results:

$$\Omega_{l,c}^2=\frac{2}{\pi}\left(\frac{8}{3}-\frac{\pi^2}{4}\right)(\Delta S)^2 Fe\frac{\cos\alpha}{\cos\theta_i\sin(\theta_i-\alpha)}R$$

(where $\theta_i\neq\alpha$) for dense columns, which has to be compared to

$$\Omega_c^2=\frac{\pi}{2}(\Delta S)^2 Fe\frac{1}{\cos\theta_i\sin(\theta_i-\alpha)\cos_\alpha}$$

for randomly distributed columns. $\Omega_{l,c}^2=K_c\Omega_c^2$, with

$$K_c=\left(\frac{2}{\pi}\right)^2\left(\frac{8}{3}-\frac{\pi^2}{4}\right)\cos^2\alpha=0{,}0807\cos^2\alpha.$$

For spherical inclusions, we have $\Omega_{l,g}^2=K_g\Omega_g^2$, with $K_g=\frac{1}{8}$. In both cases, in the dense medium, the structure induced spreading is reduced by a factor of $1/\sqrt{K}\approx 3$.

The calculations for the columnar structure of porous silicon based on data from Ref. 13 and presented in Sec. IV B. have been performed assuming a dense columnar structure. The agreement with the TEM data confirms the validity of this approach, in contrast to calculations made for a random medium, which would overestimate the spreading in this case (porosity 66%).

More generally, if we compare measured values of the spreading $\Omega_{\exp}$ and calculated values with N and R determined by some other means, we expect to find a value between $\Omega_{c,l}$ and Ω_c in the columnar case, say $\Omega_{\exp}^2=K\cdot\Omega_c^2$. The value K, being 1 for a purely random medium and K_c (or K_g for spherical inclusions) for a chaotic medium characterized by some spatial degree of organization is a measure of the randomness, i.e., an order parameter. For a completely ordered medium, for example for columns of constant wall thickness, values of K smaller than K_c (or K_g for spheres) could be obtained, very close to 0.

Like in the ion beam channeling method where the ratio χ of the peak heights in aligned and random directions between 0 and 1 reflects the degree of order of the atoms in the layer ($\chi\sim 0$ for crystalline, $\chi=1$ for amorphous), the value of K as determined in our method is a measure of the order in the spatial distribution of nanometric inhomogeneities embedded in a thin layer.

[1] *Handbook of Modern Ion Beam Materials Analysis*, edited by J.R. Tesmer and M. Nastasi (Materials Research Society, Pittsburgh, 1995).

[2] N. Bohr, Philos. Mag. **25**, 10 (1913); **30**, 581 (1915); K. Dan. Vidensk. Selsk. Mat. Fys. Medd. **18**, 8 (1948).

[3] E. Szilágyi, F. Paszti, and G. Amsel, Nucl. Instrum. Methods Phys. Res. B **100**, 103 (1995); code DEPTH (downloadable from http://www.kfki. hu/~ionhp/doc/proidx.htm)

[4] E. Szilágyi, Nucl. Instrum. Methods Phys. Res. B **161-163**, 37 (2000).

[5] E. Szilágyi, Nucl. Instrum. Methods Phys. Res. B **183**, 25 (2001).

[6] I.B. Khaibulin, G.G. Zakirov, M.M. Zaripov, T. Lohner, L. Pogány, G. Mezey, M. Fried, E. Kótai, F. Pászti, A. Manuaba, and J. Gyulai, Phys. Status Solidi A **94**, 371 (1986).

[7] M. Yesil, W. Assmann, H. Huber, and K.E.G. Löbner, Nucl. Instrum. Methods Phys. Res. B **136-138**, 623 (1998).

[8] R. Behrisch, S. Grigull, U. Kreissig, and R. Grötzschel, Nucl. Instrum. Methods Phys. Res. B **136-138**, 628 (1998).

[9] T. Sjavaara, K. Arstila, A. Laaksoo, and J. Keinonen, Nucl. Instrum. Methods Phys. Res. B **161**, 235 (2000).

[10] F. Besenbacher, J.U. Andersen, and E. Bonderup, Nucl. Instrum. Methods **168**, 1 (1980).

[11] Y. Itoh, T. Maeda, T. Nakajima, A. Kitamura, N. Ogiwara, and M. Saidoh, Nucl. Instrum. Methods Phys. Res. B **117**, 161 (1996).

[12] J.P. Stoquert, J.C. Oberlin, C. Heitz, J. Cailleret, and G. Lagarde, Nucl. Instrum. Methods Phys. Res. **188**, 249 (1981).

[13] G. Amsel, E. d'Artemare, G. Battistig, V. Morazzani, and C. Ortega, Nucl. Instrum. Methods Phys. Res. B **122**, 99 (1997).

[14] F. Pászti and E. Szilágyi, Vacuum **50**, 451 (1998).

[15] F. Pászti, E. Szilágyi, Z.E. Horváth, A. Manuaba, G. Battistig, Z. Hajnal, and É. Vázsonyi, Nucl. Instrum. Methods Phys. Res. B **136-138**, 533 (1998).

[16] Z. Hajnal, E. Szilágyi, F. Pászti, and G. Battistig, Nucl. Instrum. Methods Phys. Res. B **118**, 617 (1996).

[17] J.F. Ziegler and V. Littmark, *Handbook of Stopping Cross-sections for Energetic Ions in All Elements* (Pergamon Press, New York, 1980); J.F. Ziegler, *The Stopping and Range of Ions in Solids* (Pergamon Press, New York, 1985).

[18] M.S. Livingston and H.A. Bethe, Rev. Mod. Phys. **9**, 245 (1937).

[19] J. Lindhard and M. Scharff, K. Dan. Vidensk. Selsk. Mat. Fys. Medd. **27**, 15 (1953).

[20] E. Bonderup and P. Hvelplund, Phys. Rev. A **4**, 562 (1971).

[21] W.K. Chu, Phys. Rev. A **13**, 2057 (1976).

[22] Q. Yang, D.J. O'Connor, and A. Wang, Nucl. Instrum. Methods Phys. Res. B **61**, 149 (1991).

[23] T. Szörényi, J.-P. Stoquert, J. Perrière, F. Antoni, and E. Fogarassy, Diamond Relat. Mater. **10**, 2107 (2001).

[24] O. Geszti, G. Radnóczi, I. Bertóti, T. Szörényi, F. Antoni, and E. Fogarassy, Appl. Surf. Sci. **186**, 502 (2002).

[25] C. Ortega, J. Siejka, and G. Vizkelethy, Nucl. Instrum. Methods Phys. Res. B **45**, 622 (1990).

[26] S. Kumar, J.V. Ramana, C. David, and V.S. Raju, Nucl. Instrum. Methods Phys. Res. B **179**, 113 (2001).